Morphing of soft structures driven by active swelling: a numerical study

Ivan Colorado Cervantes[a], Michele Curatolo[b], Paola Nardinocchi[c,*], Luciano Teresi[a]

[a] *Dipartimento di Matematica e Fisica, Università Roma Tre, I-00146 Roma, Italy*
[b] *Dipartimento di Architettura, Università Roma Tre, I-00154 Roma, Italy*
[c] *Dipartimento di Ingegneria Strutturale e Geotecnica Sapienza Università di Roma, I-00184 Roma, Italy*

Abstract

The study aims to highlight the differences between growth-by-diffusion, based on the elastic stretch of the polymeric network, and growth-by-activity, based on the remodeling of the network, in polymer gels. The study is based on a multiphysics continuum model, which allows to describe the interactions between mechanics, diffusion and growth through a system of nonlinear partial differential equations. We discuss the differences between growth-by-diffusion and growth-by-activity and evidence the role of the corresponding characteristic times in the case of homogeneous activation source. We also show as a huge variety of three-dimensional shapes can be generated by controlling the distribution of the activation sources.

Keywords: bulk contraction, active gels, stress-diffusion, mechanics.

1. Introduction

Active gels are an inspiration for the development of biomimetic active materials from components that act as local stress or strain actuators. The combination of activity and elasticity can open to new technological applications which can also be supported by 4D printed techniques. Nevertheless, active gels remain largely unexplored and more experiments and more models are needed to discover and discuss their actuation performances.

In designing-actuation-by-modeling, Nature is a great source of inspiration as it offers a wide range of situations where the synergy between activity and elasticity produces impressive effects [1, 2, 3, 4, 5]. In [5], a study on leaves growing on a liquid substrate or in absence of it is presented and it is shown how the morphology of the leaf strongly

*Corresponding Author: P. Nardinocchi, Dipartimento di Ingegneria Strutturale e Geotecnica, via Eudossiana 18, I-00184 Roma, tel: 0039 06 44585242, fax: 0039 06 4884852.

Email addresses: ivan.ccervantes@gmail.com (Ivan Colorado Cervantes), michele.curatolo@uniroma1.it (Michele Curatolo), paola.nardinocchi@uniroma1.it (Paola Nardinocchi), teresi@uniroma3.it (Luciano Teresi)

depends on the interplay between internal growth-induced residual stresses and the presence (absence) of water which works as a support for leaves and also can diffuse in the leaves.
On the other hand, Technology continues its improvement by mimicking and also exceeding Nature. In [6, 7, 8], internally driven contractile gels have been generated by polymerizing actin in the presence of cross-linker and clusters of myosin as molecular motors. Successive experiments have suggested how boundaries affect morphing [6], how three-dimensional shapes can be driven from flat active gel sheets [8] and how mechanics of the sheets is affected by activation intensity [9], measured by molecular motor concentration.
The studies above inspired the analysis we present and discuss here which aims to highlight the differences between growth-by-diffusion and growth-by-activity, which is sketched in the cartoon in figure 1. Shortly, activity acts on the actin filaments and changes the chain free lengths by remodeling the reference network; on the other side, diffusion elastically stretches the chains by swelling the remodeled network. Based on a continuum model of remodeling and diffusion recently presented and discussed by some of the Authors [10, 11, 12], based on the multiplicative decomposition in an elastic and an active component of the deformation gradient, we explore the morphing of soft structures, in the form of plate-like three-dimensional bodies. Actuation of homogeneous bodies is firstly discussed to evidence the key differences between growth-by-diffusion and growth-by-activity. Then, we consider inhomogeneous bodies in the form of assemblies of two components with different levels of activity. We demonstrate with numerical simulations performed in Comsol multiphysics as differential growth-by-activity causes a geometric incompatibility resolved by curving. Differently from what occurs in passive gels under growth-by-swelling, the composite structure curves to accomodate the geometric mismatch until a stress-free shape is produced. We also show as tuning the intensity of activation source leads to get an extreme morphing which couldn't be produced without remodeling the network.
In the end, the study aims to provide an interpretation of some interesting morphologies which can be found in Nature [5], to suggest further experiments to produce the extreme actuation performances which can be attained by active gels, and to evidence a few open issues which would be worthy of attention.

2. Passive and active homogeneous gels

We start from reviewing a few basic aspects of the swelling exhibited by both passive and active gels: a gel placed in a liquid changes its volume by absorbing or desorbing the liquid and eventually reaches thermodynamic equilibrium; for active gels, an external source is needed to maintain this equilibrium.

For now, we focus on the change in volume suffered by gels, which are considered constraint-free, unloaded and at a steady state. Let us introduce the key volume ratios:

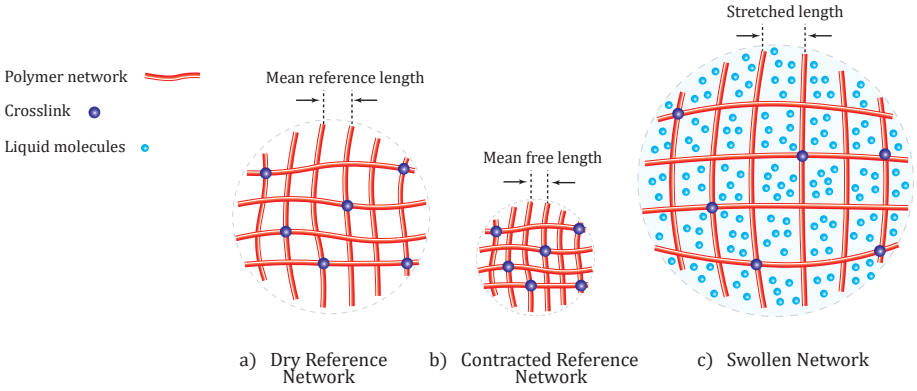

Figure 1: The characteristic states of an active gel. a) Dry-reference state of the polymer network (red) with crosslinks (blue dots). b) Dry-contracted network: mean free-length is reduced and polymer chains are still un-stretched whereas the crosslink density has changed. c) Swollen state: liquid molecules (blue dots) swell the dry-contracted network.

$$J_d = \frac{\text{swollen volume}}{\text{dry volume}}, \quad J_a = \frac{\text{remodeled volume}}{\text{dry volume}}, \quad J_e = \frac{J_d}{J_a} = \frac{\text{swollen volume}}{\text{remodeled volume}}. \tag{2.1}$$

As the dry volume is the volume of the continuum occupied by the polymer, the polymer fraction is given by $1/J_e$; the classical model for passive gel is recovered by setting $J_a = 1$. Within the Flory-Rehner thermodynamics, we consider the free-energy density per unit dry volume:

$$\psi_d = J_a\,\psi_m(\mathbf{C}_e) + J_a\,\psi_c(J_e) - p\,(J_d - \hat{J}_d). \tag{2.2}$$

In (2.2), ψ_m is the Neo-Hookean elastic energy per unit remodeled volume. Denoted with $\mathbf{F}_d$ the deformation gradient, and with $\mathbf{F}_a$ the remodeling tensor, $\mathbf{F}_e = \mathbf{F}_d\,\mathbf{F}_a^{-1}$ is the elastic deformation and $\mathbf{C}_e = \mathbf{F}_e^T\,\mathbf{F}_e$ the elastic strain. We assume:

$$\psi_m(\mathbf{C}_e) = \frac{1}{2} G_d\,(\mathbf{C}_e \cdot \mathbf{I} - 3)\,. \tag{2.3}$$

On the other side, ψ_c is the mixing energy density per unit remodeled volume, which can be written in terms of the polymer fraction $1/J_e$ as:

$$\psi_c(J_e) = \frac{RT}{\Omega}\left(\underbrace{(J_e - 1)\,\ln\!\left(\frac{J_e - 1}{J_e}\right)}_{\text{entropic}} + \underbrace{\chi\,\frac{J_e - 1}{J_e}}_{\text{enthalpic}} \right). \tag{2.4}$$

Finally, the last summand in (2.2) is the enforcement of the volumetric constraint which maintains the volume change $J = \det \mathbf{F}_d$, due to displacement, equal to the volume change $\hat{J}(c_d, J_a) = J_a + \Omega c_d$, due to the contribution of the remodeling, measured by J_a, and of the solvent, measured through the solvent molar concentration c_d ($[c_d]$ =mol/m^3) times the molar volume Ω ($[\Omega]$ =m^3/mol) of the solvent.

In (2.2) there are only three materials parameters, which are the molar volume Ω, the dis-affinity χ between solvent and polymer that is a non-dimensional parameter called Flory parameter and the shear modulus G_d of the gel measured at dry state ($[G_d] = \mathrm{J/m^3}$). Actually, it is important the ratio $\varepsilon = (G_d\,\Omega)/(\mathcal{R}\,T)$ between the elastic energy density, represented by G_d, and the chemical energy density $\mathcal{R}\,T/\Omega$, where $\mathcal{R}$ (J/(K mol) is the universal gas constant, and T (K) the temperature.

From (2.2), we obtain the prescriptions for the reference stress $\mathbf{S}_d$ and the chemical potential μ:

$$\mathbf{S}_d = \hat{\mathbf{S}}(\mathbf{F}_d, \mathbf{F}_a) - p\,\mathbf{F}_d^{\star} \quad \text{and} \quad \mu = \hat{\mu}(J_e) + p\Omega\,, \tag{2.5}$$

with

$$\hat{\mathbf{S}}(\mathbf{F}_d, \mathbf{F}_a) = G\,\mathbf{F}_e\,J_a\,\mathbf{F}_a^{-T} \quad \text{and} \quad \hat{\mu}(J_e) = R\,T\,\left[\log\left(\frac{J_e-1}{J_e}\right) + \frac{\chi + J_e}{J_e^2}\right]. \tag{2.6}$$

Moreover, from the dissipation inequality we obtain a representation of the solvent flux $\mathbf{h}_d$:

$$\mathbf{h}_d = -\mathbf{D}_d\,\nabla\left(\hat{\mu}(J_e) + p\,\Omega\right), \quad \text{with} \quad \mathbf{D}_d = \frac{D\,c_d}{R\,T}\,(\mathbf{F}_d^T\,\mathbf{F}_d)^{-1} \tag{2.7}$$

the diffusion tensor ($[\mathbf{D}_d] = \mathrm{mol^2/(J\ m\ s)}$), and D ($\mathrm{m^2/s}$) the diffusivity constant. Finally, we get the Eshelby tensor $\hat{\mathbf{E}}$, that can be represented as the sum of a mechanical $\hat{\mathbf{E}}_m$ and a chemical $\hat{\mathbf{E}}_c$ contribution

$$\hat{\mathbf{E}} = \hat{\mathbf{E}}(c_d, \mathbf{F}_d, \mathbf{F}_a, p) = \hat{\mathbf{E}}_m(\mathbf{F}_d, \mathbf{F}_a, p) + \hat{\mathbf{E}}_c(c_d, J_a, p)\,, \tag{2.8}$$

with

$$\hat{\mathbf{E}}_m(\mathbf{F}_d, \mathbf{F}_a, p) = J_a\psi_m\,\mathbf{I} - \mathbf{F}_e^T\,\mathbf{S}_d\,\mathbf{F}_a^T\,, \quad \hat{\mathbf{E}}_c(c_d, J_a, p) = (J_a\psi_c - c_d\,\mu)\,\mathbf{I}\,. \tag{2.9}$$

It is worth noting that

$$\mathbf{F}_e^T\,\mathbf{S}_d\,\mathbf{F}_a^T = 2J_a\mathbf{C}_e\frac{\partial\psi_m}{\partial\mathbf{C}_e}\,. \tag{2.10}$$

In Literature, the quantity $\mathbf{S}^M = \mathbf{C}_e\partial\psi_m/\partial\mathbf{C}_e$ is known as Mandel stress and it can be shown that in isotropic material, Mandel stress is symmetric as $\mathbf{C}_e$ and $\partial\psi_m/\partial\mathbf{C}_e$ are coaxial. Then, $\hat{\mathbf{E}}$ is a symmetric tensor.

2.1. Passive homogeneous gels

Energy (2.2) with $J_a = 1$ describes passive gels. Let us consider a homogeneous circular gel plate $\mathcal{C}_d$ with dry-reference radius and thickness r_d and h_d (and dry-volume V_d) placed in a bath of chemical potential μ_o. In this simple context, the state of the gel is completely described by J_d: the stress–free swollen state $\mathcal{C}_o$ has radius and thickness $(J_d^{1/3})r_d$ and $(J_d^{1/3})h_d$. The change in volume J_d is entirely due to the liquid uptake, that is,

$$J_d = \hat{J}_d(1, c_d) = 1 + \Omega\,c_d\,, \tag{2.11}$$

corresponding to take $J_a = 1$. So, a dry gel of volume V_d soaks up a liquid volume $V_l = \Omega\, c_d\, V_d = (J_d - 1)\, V_d$. The evolution of J_d towards the thermodynamical equilibrium is governed by the diffusion time $\tau_d = l^2/D$, where $l = r_d$ or $l = h_d$, depending on the aspect ratio h_d/r_d[1]. The steady state, that is the thermodynamic equilibrium, is attained after a time $\tau_e \gg \tau_d$, when all the fields have attained their steady values.

In this situation, it can be shown that the equilibrium value J_d is determined by solving for p the equation $\mathbf{S}_d = 0$ in $(2.5)_1$, and inserting this value in the equation of chemical equilibrium $(2.5)_2$, which can be written as

$$F(J_d; \varepsilon, \chi) = \frac{\mu_o}{\mathcal{R}\,T} = \bar{\mu}_o\,, \tag{2.12}$$

with

$$F(J_d; \varepsilon, \chi) = \varepsilon J_d^{-1/3} + \log\frac{J_d - 1}{J_d} + \frac{1}{J_d} + \frac{\chi}{J_d^2}\,. \tag{2.13}$$

Equations (2.12)-(2.13) show that liquid uptake can be controlled by $\bar{\mu}_o$ and depends on the two parameters ε and χ. As an example, for a typical hydrogel [13] in a water bath, we have $G_d = 10^4$ Pa, $\chi = 0.4$, $\Omega = 1.8 \cdot 10^{-5}$ m^3/mol, and at ambient temperature $T = 293$ K we get $\varepsilon = 7.4 \cdot 10^{-7}$. At $\mu_o = \bar{\mu}_o = 0$ J/mol, the change in volume from the dry $\mathcal{C}_d$ to the swollen state $\mathcal{C}_o$ is $J_d = 77.6$, that is, the swollen volume is 77.6 times the dry volume.

2.2. Active homogeneous gels

The description of the physics of active gels needs one more balance law [10], which, in the simplest case, govern the state variable J_a, and involves an activation source β that controls the state evolution.

For active gels, the change in volume J_d is due to both $\Omega\, c_d$ and J_a, as already written, and the gel state is described by J_d and J_a. The evolution of J_d and J_a towards the thermodynamical equilibrium is governed also by the remodeling time $\tau_m = m\,\Omega/\mathcal{R}\,T$ other than by τ_d, with m (J s/m^3) the resistance of the gel to remodel. Moreover, active gels have one more control, the activation source β (J/m^3) which drives the changes of their ground states. This source is meant to represent in our continuum model, that is, at the macroscale, the effects of the molecular motors acting at the microscale. In the model, we assume that it evolve towards a final constant value β_f which is attained at the time τ_β.

When we look at the solution for $t \simeq \tau_e \gg \tau_m, \tau_d$, the fields J_a and J_d have attained their thermodynamical equilibrium values. In this situation, it can be shown that the equilibrium solution of the problem is given by the chemical equilibrium equation (2.12), rewritten in terms of J_e as

$$F(J_e; \varepsilon, \chi) = \bar{\mu}_o\,, \tag{2.14}$$

[1]For $h_d/r_d << 1$, the characteristic length is determined by h_d; on the contrary, for $h_d/r_d >> 1$, the characteristic length is determined by r_d.

and by the balance of remodeling actions[2], which can be written as

$$J_a\Big(\frac{3}{2}\varepsilon(J_e^{2/3}-1)+(J_e-1)\log\frac{J_e-1}{J_e}+\chi(1-\frac{1}{J_e})-(J_e-1)F(J_e;\varepsilon,\chi)\Big)=\bar{\beta}\,, \quad (2.15)$$

with $\bar{\beta}=\beta/(\mathcal{R}\,T/\Omega)$ the non dimensional activation source. By using (2.14) and (2.15), this last equation simplifies in

$$J_a\Big(\frac{3}{2}\varepsilon(J_e^{2/3}-1)+\frac{J_e-1}{J_e}\Big(\frac{J_e-1}{J_e}\,\chi-1\Big)-\varepsilon(J_e-1)J_e^{-1/3}\Big)=\bar{\beta}\,. \quad (2.16)$$

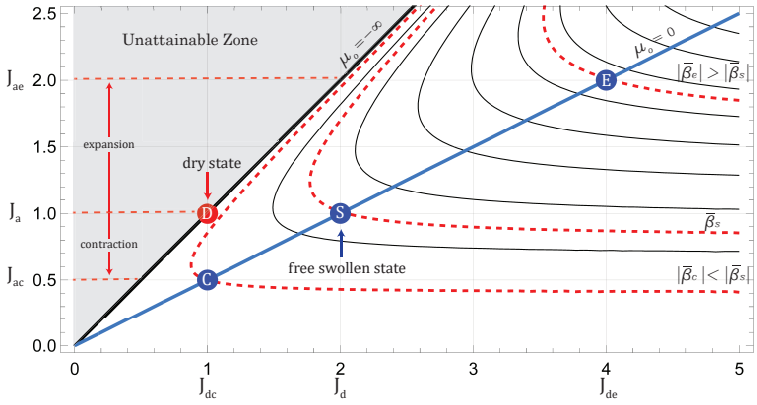

Figure 2: Swelling-contraction diagram. Steady and stress-free states at constant $\bar{\mu}_o$ lie on the line $J_a = J_e\,J_d$ with J_e determined by $\bar{\mu}_o$ through equation (2.14)). For $\bar{\mu}_o = -\infty$ we have $J_e = 1$ and thus the line $J_a = J_d$ corresponds to dry states. In the diagram, the dry state at $J_a = 1$ is identified by a red dot; blue dots identify three free-swollen states on the line $\bar{\mu}_o = 0$ maintained by different activation sources $\bar{\beta}$: as an example, S (blue) is the free-swollen state corresponding to $\bar{\mu}_o = 0$ and $\bar{\beta} = \beta_s$.

The important class of homogeneous, steady and stress-free states can be represented in the plane (J_d, J_a) through the *swelling-contraction diagram*, introduced in [10] and successively exploited in [11, 12]. These states are controlled by the (dimensionless) chemical potential $\bar{\mu}_o$ and activation source $\bar{\beta}$: to each pair $(\bar{\mu}_o, \bar{\beta})$ there corresponds a point (J_d, J_a) in the swelling-contraction diagram. The isolines of (2.14) and (2.16) yield a clue on the effects of these two controls: the states at constant $\bar{\mu}_o$ lie on the line $J_a = J_d/J_e$ with J_e determined by $\bar{\mu}_o$, while the states at constant $\bar{\beta}$ lie on a hyperbola whose asymptotes are the line $J_a = 0$ and $J_a = J_d$, represented as a black line in figure 1. For $(\bar{\mu}_o, \bar{\beta}) \to (-\infty, 0)$ we have the line $J_a = J_d$, corresponding to dry states, with the change in volume J_d only driven by activation.
Equation (2.16) reveals that, within this continuum model, any swollen state with $\bar{\mu}_o > -\infty$ requires a bulk source $\bar{\beta} \neq 0$ to remain steady.

Back to our previous example, equation (2.14) delivers $J_e = 77.6$ when $\bar{\mu}_o = 0$. From equation (2.16), it follows that to maintain $J_a = 1$ we need $\bar{\beta} = -8 \cdot 10^7\,\mathcal{R}\,T/\Omega = -0.5$,

[2]See [10, 11, 12] for details.

that is, the value corresponding to $\bar{\beta}_s$ in the figure. As expected, we also measure the same amount of total stored energy in the passive and active gel bodies when $J_a = 1$ and the visible change in volume J_d is the same. Indeed, given the function

$$\psi(J_d;\varepsilon,\chi) = \frac{\mathcal{R}\,T}{\Omega}\Big(\frac{3}{2}\varepsilon(J_d^{2/3}-1) + (J_d-1)\log\frac{J_d-1}{J_d} + \chi\frac{J_d-1}{J_d}\Big)\,, \tag{2.17}$$

which is the energy density per unit dry volume in passive gels suffering volumetric deformations, when active gels are considered, the energy density ψ_d is

$$\psi_d = J_a\psi(J_e;\varepsilon,\chi)\,, \tag{2.18}$$

and for $J_a = 1$ and $J_e = J_d$ the two energy densities are the same. The total stored energy takes the value $\Psi \simeq (-8\cdot 10^7)V_d$ J which is almost completely due to the mixing part of the free energy. It is worth noting that equation (2.18) says that the value of ψ changes with J_a: the value of Ψ stored in the deformation process, as well as the final value J_d of swollen volume, linearly change with J_a.

3. Transient states of homogeneous active gels

We discuss a few issues related to the time evolution of the state of active homogeneous gels. The idea is to discuss a few noteworthy solutions of the equations which drive the evolution of the state of active gels and to send back to the appropriate references [10, 11, 12] for details about the origin of those equations.
The time evolution of J_a and J_d which describe the state of homogeneous active gels is driven by a remodeling equation and a diffusion equation, coupled with the balance of forces equation which is always used in its quasi-static form, that is, neglecting the contribution of inertial forces.[3] Following the style of the previous section, we only focus on the time rate of active J_a and visible J_d changes in volume.
The time rate $\dot{J}_a$ is governed by a remodeling equation which takes the form

$$\tau_m\frac{\dot{J}_a}{J_a} = \bar{\beta} - J_a\Big(\frac{1}{2}(\varepsilon(J_e^{2/3}-3) + \frac{J_e-1}{J_e}\Big(\frac{J_e-1}{J_e}\,\chi - 1\Big) + \bar{p}\Big)\,, \tag{3.19}$$

where $\bar{p}$ is the reactive pressure which maintains the volumetric constraint. On the other hand, the diffusion equation can be written, by exploiting the volumetric constraint, in the form

$$\dot{J}_d = \dot{J}_a + D\mathtt{div}\left[(J_d - J_a)J_d^{-2/3}\nabla(\bar{\mu}+\bar{p})\right], \tag{3.20}$$

where

$$\bar{\mu} = \log\frac{J_e-1}{J_e} + \frac{1}{J_e} + \frac{\chi}{J_e^2}\,. \tag{3.21}$$

[3] The derivation of the three equations and the origins of their coupling have been largely discussed in the papers cited above.

Finally, the balance of forces must hold at any time and prescribe that the dimensionless reference Piola-Kirchhoff spherical stress $\mathbf{S}_d = \sigma\mathbf{I}$ must be balanced, that is,

$$\nabla\bar{\sigma} = \mathbf{0} \quad \text{with} \quad \bar{\sigma} = \varepsilon\, J_d^{1/3}(J_a^{1/3} - J_d^{1/3}\bar{p})\,, \tag{3.22}$$

under zero boundary traction. The solution $(J_a, J_d, \bar{p})$ of the problem comes from solving the equations (3.19)-(3.22) with the appropriate boundary conditions. Assuming free-embedding of the body in a bath of chemical potential $\bar{\mu}_o$, we set

$$\bar{\sigma} = 0 \quad \text{and} \quad \bar{\mu} + \bar{p} = \bar{\mu}_o\,, \tag{3.23}$$

on the boundary $\partial\mathcal{C}_d$, corresponding to have zero traction and assigned chemical potential, respectively. Finally, initial conditions for the triplet $(J_a, J_d, \bar{p})$ have to be considered.[4]
On the other hand, at equilibrium also $\dot{J}_d = 0$ and we get $\bar{\mu}+\bar{p}$ equal to a constant value which is determined by the boundary condition $(3.23)_2$.

Flory parameter	$\chi = 0.4$
Water molar volume	$\Omega = 1.8 \times 10^{-5}$ m^3/mol
Temperature	$T = 293$K
Resistance to remodeling	$m = 10^6$ Js/m^3
Shear modulus	$G_d \in [10^3, 10^5]$ Pa
Temperature	$T = 293$K
Diffusivity	$D \in [10^{-4}, 10^{-2}]$ m^2/s

Table 1: Values of parameters used in numerical experiments.

Even if homogeneous, the problem is usually numerically solved and we can stress a few issues by looking at the dependence of the numerical solutions represented in figure 3 on some key parameters such as the diffusivity D, which determines the time τ_d, and the time τ_β which determines how fast the activation source gets its final value. The other parameters have been assigned as in Table 1 with $G_d = 10^3$ Pa. Finally, it is assumed $r_d = 1.5$ mm and $h_d = 0.4\, r_d$.

Firstly, figure 3 (left) shows as the change in volume J_a (solid lines) due to remodeling strictly follows the time pattern of the activation source[5] $\bar{\beta}$ (marked lines), independently on τ_β which is chosen equal to $5\cdot10^2$ s (blue), $5\cdot10^3$ s (green) and $5\cdot10^4$ s (red). Actually, if we introduce the dimensionless time $\tau = t/\tau_\beta$ and rewrite equation (3.19) as

$$\frac{\tau_m}{\tau_\beta}\frac{d}{d\tau}J_a = J_a\bar{\beta} - J_a^2\Big(\frac{1}{2}(\varepsilon(J_e^{2/3} - 3) + \frac{J_e - 1}{J_e}\Big(\frac{J_e - 1}{J_e}\,\chi - 1\Big) + \bar{p}\Big)\,, \tag{3.24}$$

[4]It is worth noting that equation (2.16) comes from the equation (3.19) assuming that $\dot{J}_a = 0$ and $\bar{p} = \varepsilon\, J_e^{-1/3}$, as a consequence of the equations (3.23) and (3.22).

[5]Note that there are two different vertical scales in the panel.

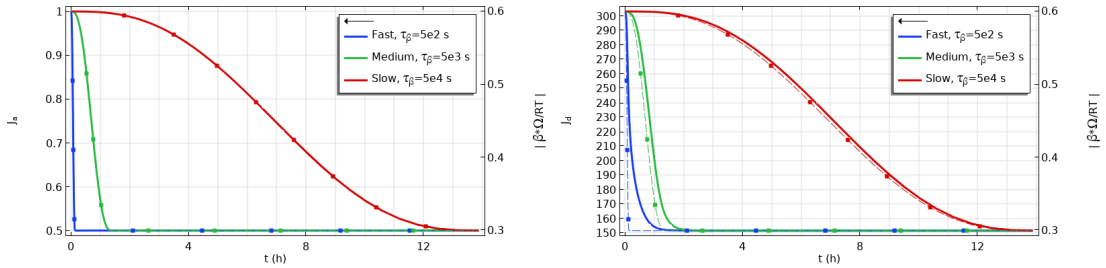

Figure 3: Effects of remodeling time τ_β (measured in hours) at constant diffusivity $D = 10^{-3}$ m^2/s. Left) J_a (solid) and $\bar{\beta}$ (markers) versus time for three values of τ_β: $\tau_\beta = 5 \cdot 10^2$ s (blue), $\tau_\beta = 5 \cdot 10^3$ s (green) and $\tau_\beta = 5 \cdot 10^4$ s (red); the remodeled volume J_a is superimposed to the remodeling action $\bar{\beta}$ for each value of τ_β. Right) J_d (solid) and $\bar{\beta}$ (markers) versus time for three values of τ_β: the evolution of the swollen volume J_d might have a delay due to the diffusion of the solvent within the gel. For both plots, values of $\bar{\beta}$ are at right y-axis.

we note that when we look at the solution for $t \ll \tau_e$ and $\tau_m/\tau_\beta << 1$, we can approximate the dynamical process governed by the equation (3.24) as a sequence of equilibrium states by assuming $\tau_m/\tau_\beta dJ_a/d\tau \simeq 0$. The sequence of equilibrium problems we solve is controlled by $\bar{\beta}$ and says that, at any time, the active change in volume $J_a \propto \bar{\beta}$ with the proportionality factor depending on the solution $(J_e, \bar{p})$ of the equations (3.20)-(3.22). This is exactly what figure 3 shows, as in our case τ_m/τ_β varies from 10^{-6} (for $\tau_\beta = 5 \cdot 10^2$ s) to 10^{-8} (for $\tau_\beta = 5 \cdot 10^4$ s).
Secondly, figure 3 (right) shows that the time evolution of J_d (solid lines) is slightly delayed with respect to the time evolution of $\bar{\beta}$, even if the delay is more evident when τ_β is smaller. On the other hand, figure 4 (left) shows as for $\tau_\beta = 5 \cdot 10^3$ s, the delay decreases if the diffusivity constant increases, so decreasing the diffusion time τ_d. Indeed, a qualitative analysis of the equation (3.20) says that the time evolution of J_d is damped with respect to J_a by the diffusion which is less effective in case of fast diffusion, as the second addend in the right side of the equation (3.20) shows.

Finally, figure 4 (right) shows as following the curve J_a versus J_d in the swelling-contraction diagram during the time evolution, we can go from an initial state $(J_{ao} = 1, J_{do} = 303)$ towards the final state $(0.5, 150)$ following an equilibrium path (red line) for high values of τ_β ($\tau_\beta = 5 \cdot 10^4$ s) or staying far (green line) or very far (blue line) for medium values of τ_β ($\tau_\beta = 5 \cdot 10^3$ s) and for small values of τ_β ($\tau_\beta = 5 \cdot 10^2$ s), respectively.
In any case, the final state is not affected by the time rate of the activation source but only by its final value which is taken always equal to $\bar{\beta}_f$.

3.1. Time-rate dependent final state

Following the evolution of the changes in volume J_a and J_d does not explain how active gels can get final states, which depend on the time-rate of the activation source. To discuss this delicate point, which makes the active gel like a material with memory of the load (activation source) history, it is mandatory to exploit the evolution of the growth tensor $\mathbf{F}_a$ and not only of its volumetric component determined by J_a.

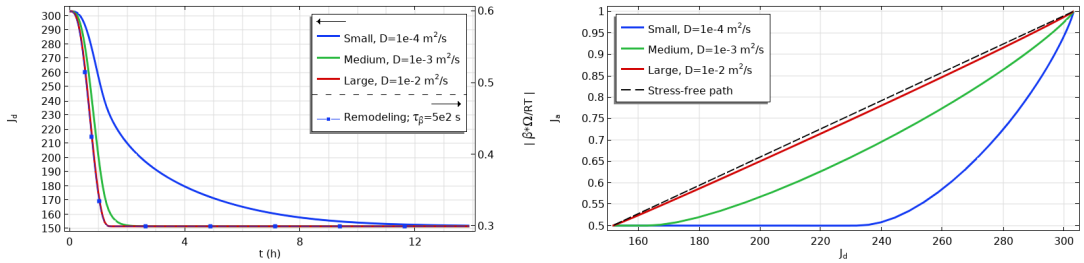

Figure 4: Effects of diffusivity D at constant $\tau_\beta = 5 \cdot 10^2$ s. Left) J_d (solid) and $\bar{\beta}$ (markers) versus time for three values of diffusivity D: $D = 1 \cdot 10^{-4}$ m^2/s (blue), $D = 1 \cdot 10^{-3}$ m^2/s (green) and $D = 1 \cdot 10^{-2}$ m^2/s (red); the smaller the diffusivity, the larger the delay between the remodeling action $\bar{\beta}$ and the swollen volume J_d. The values of $\bar{\beta}$ are at right y-axis. Right) Swelling-contraction diagram showing J_a versus J_d during the time evolution for three different values of diffusivity D. The smaller the diffusivity, the larger the difference between the actual paths (solid) and the stress-free path (dashed) represented by a straight line joining the initial state to the final one.

We stress the issue with reference to the circular gel disk $\mathcal{C}_d$ which is activated and swell under axisymmetric cylindrical conditions.[6] Under these hypotheses, we assume $\mathbf{u} = (u_r, 0, u_\zeta)$. Moreover, the deformation tensor $\mathbf{F}_d$ and the stress tensor $\mathbf{S}_d$ take in the cylindrical basis the form:

$$\mathbf{F}_d = \begin{bmatrix} 1 + u_{r,r} & 0 & u_{r,\zeta} \\ 0 & \frac{u_r}{r} & 0 \\ u_{\zeta,r} & 0 & u_{\zeta,\zeta} \end{bmatrix} \quad \text{and} \quad [\mathbf{S}_d] = \begin{bmatrix} S_{rr} & S_{r\theta} & S_{r\zeta} \\ 0 & S_{\theta\theta} & 0 \\ S_{\zeta r} & S_{\zeta\theta} & S_{\zeta\zeta} \end{bmatrix}. \tag{3.25}$$

$\mathbf{u} = (u_r, 0, u_\zeta)$ According to the axisymmetric cylindrical hypothesis and taking into account the issues discussed in [14], we assume the following symmetric representation of the growth tensor $\mathbf{F}_a$:[7]

$$\mathbf{F}_a = \begin{bmatrix} \gamma_r & 0 & \gamma_{r\zeta} \\ \cdot & \gamma_\theta & 0 \\ \cdot & \cdot & \gamma_\zeta \end{bmatrix}. \tag{3.26}$$

The choice (3.26) corresponds to assume that the rotational component $\mathbf{R}_a$ of $\mathbf{F}_a$, delivered by the polar decomposition of $\mathbf{F}_a$, is equal to the identity and $\mathbf{F}_a \equiv \mathbf{U}_a$. and the symmetric field $\mathbf{F}_a$ has a cylindrical axisymmetric form. Under these assumptions, the balance equations of forces take the form

$$S_{rr,r} + \frac{(S_{rr} - S_{\theta\theta})}{r} + S_{r\zeta,\zeta} = 0 \quad \text{and} \quad S_{\zeta\zeta,\zeta} + S_{\zeta r,r} = 0\,. \tag{3.27}$$

[6] For details, look at Refs.[10, 11, 12].

[7] The moltiplicative decomposition of the deformation gradient in an elastic and an inelastic (here, active) active component has been largely discussed in the Literature, as it hids an indeterminacy issue about the contracted reference state (see [15, 16, 17, 18, 19].

On the other hand, the solvent flux $\mathbf{h}_d = (h_r, 0, h_\zeta)$ and the balance of solvent mass takes the form

$$\dot{c_d} = -(h_{r,r} + \frac{h_r}{r} + h_{\zeta,\zeta}\,). \tag{3.28}$$

Finally, the symmetric component of the remodeling balance equation is considered

$$\mathbf{M}\mathbf{D}_a = \beta\mathbf{I} - \hat{\mathbf{E}} \quad \text{with} \quad \mathbf{D}_a = \mathrm{sym}\,(\dot{\mathbf{F}}_a\mathbf{F}_a^{-1})\,, \tag{3.29}$$

which deliver 4 not trivial equations which govern the evolution of the scalar components $(\gamma_r, \gamma_\theta, \gamma_\zeta, \gamma_{r\zeta})$. It holds:

$$\mathbf{D}_a = \begin{bmatrix} \frac{\gamma_{r\zeta}\dot{\gamma}_{r\zeta} - \dot{\gamma}_r\gamma_\zeta}{\gamma_{r\zeta}^2 - \gamma_r\gamma_\zeta} & 0 & \frac{-\dot{\gamma}_{r\zeta}(\gamma_r+\gamma_\zeta) + \gamma_{r\zeta}(\dot{\gamma}_r+\dot{\gamma}_\zeta)}{2(\gamma_{r\zeta}^2 - \gamma_r\gamma_\zeta)} \\ \cdot & \frac{\dot{\gamma}_\theta}{\gamma_\theta} & 0 \\ \cdot & 0 & \frac{\gamma_{r\zeta}\dot{\gamma}_{r\zeta} - \gamma_r\dot{\gamma}_\zeta}{\gamma_{r\zeta}^2 - \gamma_r\gamma_\zeta} \end{bmatrix} = \begin{bmatrix} D_r & 0 & D_{r\zeta} \\ \cdot & D_\theta & 0 \\ \cdot & 0 & D_\zeta \end{bmatrix}. \tag{3.30}$$

Finally, the Eshelby tensor can be written as

$$\hat{\mathbf{E}} = (J_a(\psi_m + \psi_c) - c_d\mu)\mathbf{I} - 2J_a\mathbf{S}^M\,. \tag{3.31}$$

Then, assuming that $\mathbf{M} = m\mathbf{I}$, we get the 4 evolution equations in the form:

$$\begin{aligned} m\,D_r &= \beta - (J_a(\psi_m + \psi_c) - c_d\mu) - 2J_aS_r^M\,, \\ m\,D_\theta &= \beta - (J_a(\psi_m + \psi_c) - c_d\mu) - 2J_aS_\theta^M\,, \\ m\,D_\zeta &= \beta - (J_a(\psi_m + \psi_c) - c_d\mu) - 2J_aS_\zeta^M\,, \\ m\,D_{r\zeta} &= -2J_aS_{r\zeta}^M\,. \end{aligned} \tag{3.32}$$

These equations are supplemented by boundary mechanical and chemical conditions which prescribe

$$\mathbf{S}_d\mathbf{m} = \mathbf{0} \quad \text{and} \quad \mu(J_e) + p\Omega = \mu_o\,, \tag{3.33}$$

respectively, on the boundary $\partial\mathcal{C}_d$. Finally, the initial conditions are: $\mathbf{F}_a = \mathbf{I}$, $c_d = (J_{do} - 1)/\Omega$, $u_r = (J_{do}^{1/3} - 1)r$, $u_\zeta = (J_{do}^{1/3} - 1)\zeta$.

3.2. Slow versus fast remodeling

We study the active swelling dynamics of a circular gel disk $\mathcal{C}_d$ with dry-reference radius $r_d = 1.5$ mm and thickness $h_d = 0.4\,r_d$; materials parameters are those in Table 1, with $G_d = 10^3$ Pa.

In our experiment, we assume as initial state a free-swelling state with $J_d = 303$ and $J_a = 1$, which is steady with $\bar{\mu}_o = 0$ and $\bar{\beta} = \bar{\beta}_0 = -0.60$. The remodeling is initiated by changing the value of the external remodeling source according to the law

$$\bar{\beta}(t) = \bar{\beta}_0 + (\bar{\beta}_f - \bar{\beta}_0)\,s(t/\tau_\beta), \tag{3.34}$$

with $s(.)$ a smoothed step function such that $s(0) = 0$, and $s(1) = 1$. The final value of the remodeling source is set to $\bar{\beta}_f = -0.18$, corresponding to $J_a = 0.3$ and $J_d = 90$. During the evolution, solvent is exchanged with the environment.
To explore the effect of the remodeling on the final state of the contracted gel, we consider a slow activation with $\tau_\beta = 5 \cdot 10^3$ s, and a fast one with $\tau_\beta = 50$ s.
The slow activation yields a contraction which is almost homogeneous and stress-free; the tensor $\mathbf{F}_a$ remains almost diagonal, that is $\mathbf{F}_a \simeq \gamma\,\mathbf{I}$, with $\gamma_r \simeq \gamma_\theta \simeq \gamma_z \simeq \gamma$ and $\gamma_{rz} \simeq 0$. This behavior can be appreciated in figure 5. In figure 5, left, we see the time evolution of J_d (solid, green), which shows a small delay with respect to the time evolution of $\bar{\beta}$ (dashed, green, markers). In the right panel, we show the swelling-contraction diagram; therein, the path (J_d, J_a) (solid, green) is close to the straight line representing the stress-free path (dashed, black); the three components γ_r, γ_θ, γ_z maintains the same values during the evolution (dashed, green, markers).
The fast activation yields a contraction which is far from homogeneous and quite stressed; while $\gamma_{rz} \simeq 0$, the three diagonal components of $\mathbf{F}_a$ have different values during the evolution. In figure 5, left, we see that time evolution of J_d (solid, blue) has a large delay with respect to the time evolution of $\bar{\beta}$ (dashed, blue, markers). In the right panel, the path (J_d, J_a) (solid, blue) is distant to the stress-free path (dashed, black); the three components γ_r, γ_θ, γ_z have different values during the evolution (dashed, blue, markers). The final shapes of the gel are shown in figure 6 for fast, panel a) and c), and slow, panel b) and d) remodeling time τ_β. Colour code refers to γ_ζ values in the panels a) and b) and to J_d in the panels c) and d). It can be appreciated from the figure how the not isotropic evolution of the remodeling tensor, evidenced in the right panel of figure 5, yields a not uniform final state. A noteworthy finding is that both the final states which correspond to a slow or a fast time τ_β are stress-free.

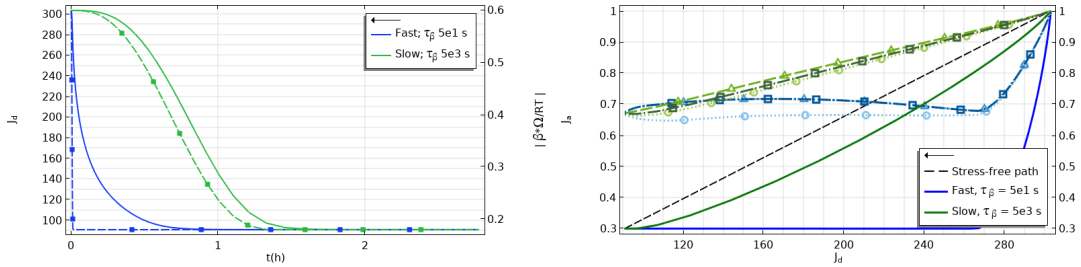

Figure 5: Left) Average J_d (solid) and $\bar{\beta}$ (dashed) versus time for fast (blue) and slow (green) remodeling time τ_β. Under fast remodeling, the swollen volume J_d lags behind the remodeling action $\bar{\beta}$. Right) Swelling-contraction diagram showing average J_a versus average J_d (solid) during the time evolution for fast (green) and slow (blue) remodeling time τ_β; the diagram shows also the path of the diagonal terms (averaged) of $\mathbf{F}_a$: γ_r (dashed, circle) γ_θ (dashed, triangle), γ_z (dashed, square). The slow path is close to the stress-free straight line (dashed, black) and the remodeling is almost isotropic. For both plots: values of $\bar{\beta}$ are at right y-axis; $\tau_\beta = 50$ s (blue), $\tau_\beta = 5 \cdot 10^3$ s (green); $D = 10^{-3}$ m^2/s.

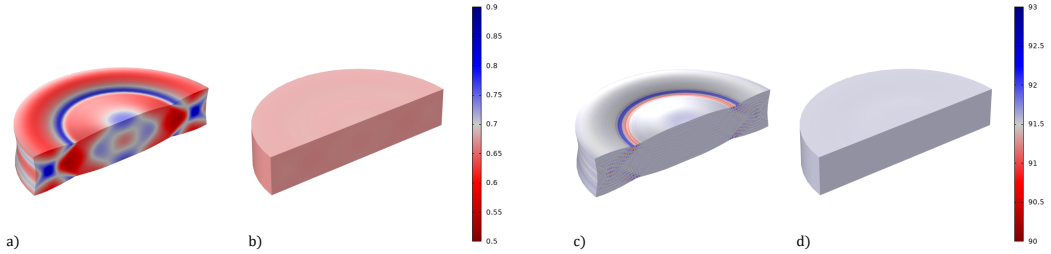

Figure 6: Final shapes of the disk corresponding to a fast a) and c) and to a slow b) and d) remodeling. Left) colour code refers to γ_ζ values. Right) colour code refers to J_d values. For fast remodeling, $\tau_\beta = 50$ s; for slow remodeling, $\tau_\beta = 5 \cdot 10^3$ s.

4. Extreme deformation of active gels under not uniform activation

Combining active gel disks differently activated, we can produce shapes that largely differ from those corresponding to the disks homogeneously activated discussed in the previous sections. To evidence the combined effects of swelling and remodeling on the morphing, we study both soft and hard gel disks. We study the active swelling dynamics of a thin disk $\mathcal{C}_d$, fixing $r_d = 1.5$ mm and $h_d = 0.05\, r_d$. The departure from the initial free-swelling state is produced by choosing a change in the bulk activation source only in the half bottom layer. Two different cases are studied: the first corresponds to an impermeable hard disk with $G_d = 10^5$ Pa which actively expands in the half bottom region; the second is a permeable soft disk with $G_d = 10^3$ Pa which actively contracts in the half bottom region. The diffusivity $D = 10^{-3}$ m^2/s and the remodeling time $\tau_\beta = 1500$ s is the same for the two layers. The other materials parameters are those in Table 1.

The remodeling is initiated by changing the value of the external remodeling source

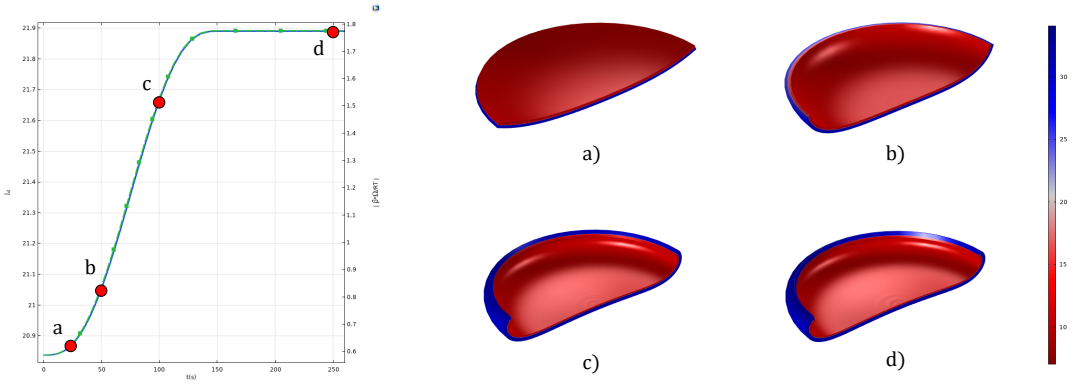

Figure 7: Hard disk under expansion at bottom half. Left) Average J_d (solid, blue) and activation source $\bar{\beta}_b$ probed at bottom (marked, green) versus time. Right) Snapshots of the shape at different stages during the evolution: $t = 25$s (a), $t = 50$s (b), $t = 100$s (c), and $t = 250$s (d), (right); color code refers to the swollen volume J_d.

according to the law $\bar{\beta}(t, z) = \bar{\beta}(t)\, s_z((z - h_d/2)\, 10/h_d)$, with $\bar{\beta}(t)$ given by (3.34) and

$s_z(.)$ a smoothed step function.
In the first case study, the initial condition of the hard disk is a stress-free swelling state with $J_d = 20.8$ and $J_a = 1$, which is steady with $\bar{\mu}_o = 0$ and $\bar{\beta} = \bar{\beta}_o = -0.59$. The final value of the remodeling source is $\bar{\beta} = \bar{\beta}_f = -1.78$, corresponding to a target final $J_a = 3$. The boundary is assumed not permeable, thus, during the evolution solvent cannot be exchanged with the environment; due to remodeling, solvent migrates from the passive top layer to the active bottom layer.
Figure 7 shows the shape change of the disk under the active expansion of the bottom layer to $J_a = 3$. The left panel shows the time-course of the average swollen volume J_d (solid, blue) and activation source $\bar{\beta}$ probed at the bottom half of the disc (marked, green). The two paths are superimposed, meaning that the remodeling is slow with respect to diffusion characteristic time. The right panel shows snapshots of the current configuration at $t = 25$ s (a), $t = 50$ s (b), $t = 100$ s (c), and $t = 250$ s (d). Expansion at the bottom drains solvent from the top half, which is drying, to the bottom half that increases its solvent content; the colour code refers to the swollen volume J_d, with red corresponding to more dry and blue to more wet. The incompatibility of the remodeling yields a curved dome-like shape, having higher curvature at the periphery. A noteworthy finding is that the final shape is steady and stress-free.
In the second case study, the initial condition of the soft disk is a stress-free swelling state with $J_d = 303$ and $J_a = 1$, which is steady with $\bar{\mu}_o = 0$ and $\bar{\beta} = \bar{\beta}_o = -0.60$. The final value of the remodeling source is $\bar{\beta} = \bar{\beta}_f = -0.30$, corresponding to a final target $J_a = 0.5$. The boundary is assumed permeable, thus, during the evolution solvent can be exchanged with the environment.
Figure 8 shows shape change of the disk under the active contraction of the bottom layer to$J_a = .5$. The left panel shows the time-course of the average swollen volume J_d (solid, blue) and activation source $\bar{\beta}$ probed at the bottom half of the disc (marked, green). The right panel shows snapshots of the current configuration at $t = 500$ s (a), $t = 1000$ s (b), $t = 1500$ s (c), and $t = 2000$ s (d). Contraction at the bottom expels solvent from this region, which is drying; meanwhile, the top half increases its solvent content; the colour code refers to the swollen volume J_d, with red corresponding to more dry and blue to more wet. As in the previous case, the incompatibility of the remodeling yields a curved dome-like shape, having higher curvature at the periphery. Also in this case, the final shape is steady and stress-free. Let us note that these solutions have been obtained under the hypothesis of cylindrical symmetry; we expect that a fully 3D solution would exhibit an hyperbolic shape instead of a parabolic one.

5. Conclusions

Active gels have all the noteworthy characteristics of the gels plus the capability to remodel their networks when appropriately activated, as shown in [8]. Typically, the double-active nature of these gels, which can change their shape due to growth-by-diffusion and growth-by-activity, makes the morphing capabilities extremely wider if compared with standard gels.
This work explore the morphing of soft active gel disks under uniform and not uniform

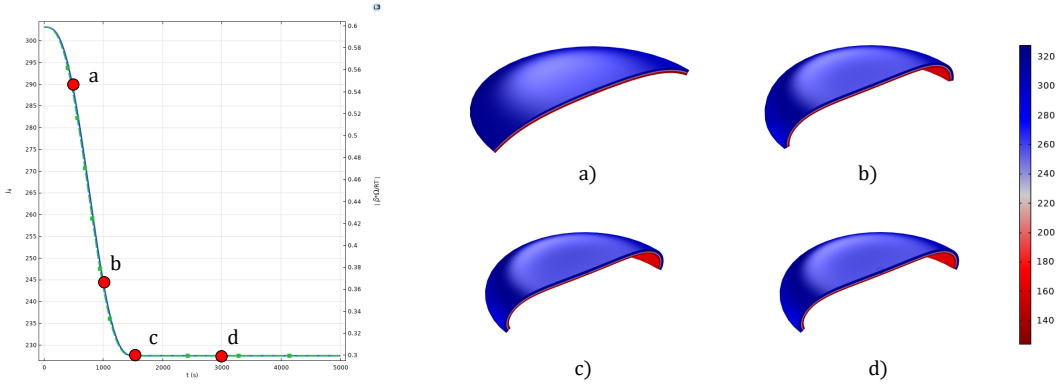

Figure 8: Soft disk under contraction at bottom half. Left) Average J_d (solid, blue) and activation source $\bar{\beta}_b$ probed at bottom (marked, green) versus time. Right) Snapshots of shape at different stages during the evolution: $t = 500$s (a), $t = 100$s (b), $t = 1500$s (c), and $t = 2000$s (d); color bar is the swollen volume J_d.

actuation, by setting up a series of numerical experiments which highlight a few key performances of the gels. As it has been shown, many parameters affect the morphing. In particular, the focus here has been on the remodeling time which depends on the time rate of the bulk activation source and may affect the final state of the active gels.

Acknowledgements

This work is supported by MIUR (Italian Ministry for Education, Research, and University) through *PRIN 2017, Mathematics of active materials: From mechanobiology to smart devices*, project n. 2017KL4EF3 and by MAECI (Italian Ministry for Foreign Affairs and International Cooperation) through *PAMM project: Microencapsulation based on intelligent actively-remodeling bio polymer gels for controlled drug release.*

References

[1] I. Burgert, P. Fratzl, Actuation systems in plants as prototypes for bioinspired devices, Philosophical Transactions of the Royal Society A: Mathematical, Physical and Engineering Sciences 367 (1893) (2009) 1541–1557. arXiv:https://royalsocietypublishing.org/doi/pdf/10.1098/rsta.2009.0003, doi:10.1098/rsta.2009.0003.
URL https://royalsocietypublishing.org/doi/abs/10.1098/rsta.2009.0003

[2] O. J. N. Bertrand, D. K. Fygenson, O. A. Saleh, Active, motor-driven mechanics in a dna gel, Proceedings of the National Academy of Sciences 109 (43) (2012) 17342–17347. arXiv:https://www.pnas.org/content/109/43/17342.full.pdf, doi:10.1073/pnas.1208732109.
URL https://www.pnas.org/content/109/43/17342

[3] L. Beauzamy, N. Nakayama, A. Boudaoud, Flowers under pressure: ins and outs of turgor regulation in development, Annals of Botany 114 (7) (2014) 1517–1533. arXiv:https://academic.oup.com/aob/article-pdf/114/7/1517/16993167/mcu187.pdf, doi:10.1093/aob/mcu187.
URL https://doi.org/10.1093/aob/mcu187

[4] Y. Bashirzadeh, A. P. Liu, Encapsulation of the cytoskeleton: towards mimicking the mechanics of a cell, Soft Matter 15 (2019) 8425–8436. doi:10.1039/C9SM01669D.
URL http://dx.doi.org/10.1039/C9SM01669D

[5] F. Xu, C. Fu, Y. Yang, Water affects morphogenesis of growing aquatic plant leaves, Phys. Rev. Lett. 124 (2020) 038003. doi:10.1103/PhysRevLett.124.038003.
URL https://link.aps.org/doi/10.1103/PhysRevLett.124.038003

[6] M. K. Matthias Schuppler, Felix C. Keber, A. R. Bausch, Boundaries steer the contraction of active gels, Nature Communications 7 (2016) 13120.

[7] A. Bernheim-Groswasser, N. S. Gov, S. A. Safran, S. Tzlil, Living matter: Mesoscopic active materials, Advanced Materials 30 (41) (2018) 1707028. arXiv:https://onlinelibrary.wiley.com/doi/pdf/10.1002/adma.201707028, doi:10.1002/adma.201707028.
URL https://onlinelibrary.wiley.com/doi/abs/10.1002/adma.201707028

[8] Y. Ideses, V. Erukhimovitch, R. Brand, D. Jourdain, J. Salmeron, Hernandez, U. Gabinet, S. Safran, K. Kruse, A. Bernheim-Groswasser, Spontaneous buckling of contractile poroelastic actomyosin sheets, Nature Communications 9 (2018) 2461.

[9] A. Sonn-Segev, A. Bernheim-Groswasser, Y. Roichman, Scale dependence of the mechanics of active gels with increasing motor concentration, Soft Matter 13 (2017) 7352–7359. doi:10.1039/C7SM01391D.
URL http://dx.doi.org/10.1039/C7SM01391D

[10] M. Curatolo, S. Gabriele, L. Teresi, Swelling and growth: a constitutive framework for active solids, Meccanica 52 (14) (2017) 3443–3456. doi:10.1007/s11012-017-0629-x.
URL https://doi.org/10.1007/s11012-017-0629-x

[11] M. Curatolo, P. Nardinocchi, L. Teresi, Dynamics of active swelling in contractile polymer gels, Journal of the Mechanics and Physics of Solids 135 (2020) 103807. doi:https://doi.org/10.1016/j.jmps.2019.103807.
URL http://www.sciencedirect.com/science/article/pii/S002250961930835X

[12] M. Curatolo, P. Nardinocchi, L. Teresi, Mechanics of active gel spheres under bulk contraction, International Journal of Mechanical Sciences 193 (2021) 106147. doi:https://doi.org/10.1016/j.ijmecsci.2020.106147.

URL https://www.sciencedirect.com/science/article/pii/S0020740320342521

[13] N. A. Peppas, Hydrogels in medicine and pharmacy: fundamentals, Vol. 1, CRC press, 2019.

[14] J. Ciambella, P. Nardinocchi, A structurally frame-indifferent model for anisotropic visco-hyperelastic materials, Journal of the Mechanics and Physics of Solids 147 (2021) 104247. doi:https://doi.org/10.1016/j.jmps.2020.104247.
URL https://www.sciencedirect.com/science/article/pii/S0022509620304580

[15] C. Eckart, The thermodynamics of irreversible processes. iv. the theory of elasticity and anelasticity, Phys. Rev. 73 (1948) 373–382. doi:10.1103/PhysRev.73.373.

[16] E. H. Lee, Elastic-Plastic Deformation at Finite Strains, Journal of Applied Mechanics 36 (1) (1969) 1–6. arXiv:https://asmedigitalcollection.asme.org/appliedmechanics/article-pdf/36/1/1/5449476/1_1.pdf, doi:10.1115/1.3564580.
URL https://doi.org/10.1115/1.3564580

[17] A. Green, P. Naghdi, Some remarks on elastic-plastic deformation at finite strain, International Journal of Engineering Science 9 (12) (1971) 1219 – 1229. doi:10.1016/0020-7225(71)90086-3.

[18] Y. F. Dafalias, Plastic spin: necessity or redundancy?, International Journal of Plasticity 14 (9) (1998) 909 – 931. doi:10.1016/S0749-6419(98)00036-9.

[19] O. T. Bruhns, The Multiplicative Decomposition of the Deformation Gradient in Plasticity—Origin and Limitations, Springer International Publishing, Cham, 2015, pp. 37–66.